

Insights into the Mechanism of Methanol Steam Reforming Tandem Reaction over CeO₂ Supported Single-Site CatalystsLuning Chen,[§] Zhiyuan Qi,[§] Xinxing Peng, Jeng-Lung Chen, Chih-Wen Pao, Xibo Zhang, Chaochao Dun, Melissa Young, David Prendergast, Jeffrey J. Urban, Jinghua Guo, Gabor A. Somorjai,* and Ji Su*Cite This: *J. Am. Chem. Soc.* 2021, 143, 12074–12081

Read Online

ACCESS |



Metrics & More

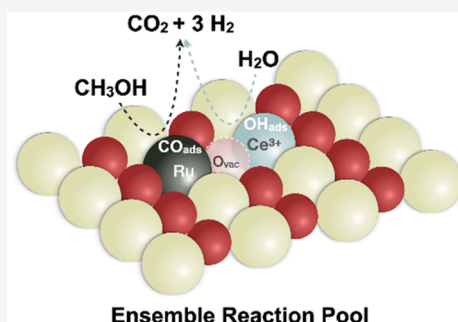


Article Recommendations



Supporting Information

ABSTRACT: We demonstrated how the special synergy between a noble metal single site and neighboring oxygen vacancies provides an “ensemble reaction pool” for high hydrogen generation efficiency and carbon dioxide (CO₂) selectivity of a tandem reaction: methanol steam reforming. Specifically, the hydrogen generation rate over single site Ru₁/CeO₂ catalyst is up to 9360 mol H₂ per mol Ru per hour (579 mL_{H₂} g_{Ru}^{−1} s^{−1}) with 99.5% CO₂ selectivity. Reaction mechanism study showed that the integration of metal single site and O vacancies facilitated the tandem reaction, which consisted of methanol dehydrogenation, water dissociation, and the subsequent water gas shift (WGS) reaction. In addition, the strength of CO adsorption and the reaction activation energy difference between methanol dehydrogenation and WGS reaction play an important role in determining the activity and CO₂ selectivity. Our study paves the way for the further rational design of single site catalysts at the atomic scale. Furthermore, the development of such highly efficient and selective hydrogen evolution systems promises to deliver highly desirable economic and ecological benefits.



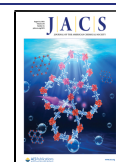
■ INTRODUCTION

Single-site catalysts, where isolated metal atoms are anchored on supports by bonding to N or O atoms, have opened up a new research frontier in the catalysis field.^{1–6} The downsizing of metal nanoparticles to a single atom can achieve the maximum efficiency of utilizing noble metals and creating more active sites.^{7–11} Isolated metal sites typically show excellent activity in many catalytic reactions involving small molecules, such as CO oxidation, water gas shift (WGS) reaction, and methane selective oxidation.^{12–14} However, the lack of ensemble sites prevents reactions that involve large molecules and some multistep reactions.^{15–17} Recent research demonstrated that “ensemble effects” between metal single atoms and neighboring oxygen vacancies can favor oxygen transfer and reactant adsorption, promoting catalytic reaction efficiency with large molecules.^{18–20} In our previous studies, we demonstrated the enhanced activity and selectivity of methanol dehydrogenation and *n*-hexane reforming when combining an oxygen vacancy with noble metal atoms.^{21–23} The mechanism study also showed that the integration of metal single-sites and neighboring oxygen vacancies creates a special synergy that accelerates the reaction rates by facilitating the adsorption and activation of reactants and the transformation of intermediate species.^{18,22} Therefore, we envisioned expanding the reaction scope to tandem reactions and studying this “ensemble effect” of single-site catalysts further.

Hydrogen plays an important role in the transition to a cleaner energy landscape.²⁴ However, the safety of hydrogen transportation and storage remains a bottleneck for the upcoming hydrogen economy.^{25,26} Storage of hydrogen in chemical bonds of liquid organic hydrogen carriers (LOHCs) provides a way to overcome this limitation. Among all the LOHCs, methanol is identified as an ideal hydrogen carrier owing to its low cost and wide availability.²⁷ However, direct methanol dehydrogenation always coproduces CO, which can poison catalysts, especially in the application of polymer electrolyte membrane fuel cells (PEMFCs).^{28,29} Methanol steam reforming (MSR), as a tandem reaction,³⁰ consists of two sequential reactions: methanol dehydrogenation (CH₃OH = CO + 2 H₂) and water gas shift (WGS) reaction (CO + H₂O = CO₂ + H₂). Therefore, the total reaction of MSR (CH₃OH + H₂O = CO₂ + 3 H₂) can not only avoid CO emissions but also generate one more stoichiometrically equivalent hydrogen.³¹ In pioneering work, α -MoC-supported, single-site Pt or Ni catalysts were discovered exhibiting extraordinary hydrogen production activity in the aqueous-phase methanol reforming

Received: April 13, 2021

Published: July 30, 2021



reaction.^{32,33} The abundant surface hydroxyls of α -MoC provide highly active sites for water dissociation, thus accelerating the tandem methanol-reforming reaction at the interface between Pt₁ and α -MoC. However, the underlying tandem mechanism of MSR over single-site catalysts has remained elusive.

The tandem reactions catalyzed by functional nanostructures have been effectively studied.^{34–37} Typically, tandem reactions occur on the surface of multifunctional material or at the interface of different functional materials.^{34,38} Our previous mechanism studies of tandem reactions found the spatial arrangement of the interfaces of tandem catalyst could control the generation, diffusion, and reaction of the intermediates, and finally favor the selectivity of desired products.³⁹ However, single-site catalysts, the logical end points of the downsizing, have distinct geometric and electronic structures. Therefore, the surface/interface reaction model that is suitable for traditional metal nanoparticle catalysts can no longer precisely describe the reaction behaviors of metal single-sites and needs to be revamped.

In this work, we studied the mechanism of tandem MSR reaction over a series of CeO₂-supported single-site catalysts (Pt₁/CeO₂, Pd₁/CeO₂, Rh₁/CeO₂, Ru₁/CeO₂). We showed that well-defined reaction sites consisting of a metal single atom and neighboring oxygen vacancies possessed unique catalytic properties. Compared to the other three single-site catalysts, Ru₁/CeO₂ displayed the highest hydrogen production rate and CO₂ selectivity. Further study indicated that superior performance could be attributed to the strong CO adsorption and suitable elementary-step reaction activity.

EXPERIMENTAL METHODS

Synthesis of M₁/CeO₂ Single-Site Catalysts (M = Ru, Rh, Pt, Pd). Porous CeO₂ nanorod support was synthesized by following the previous report.⁴⁰ The single-site M₁/CeO₂ catalysts were synthesized by an ascorbic acid (AA)-assisted reduction method according to our prior work with some modifications.²⁰ Typically, 500 mg CeO₂ was first dispersed in 175 mL of distilled water, and 1 mmol AA was added to the solution. After being stirred at room temperature for 3 h, the products were collected by centrifugation, washed with distilled water several times, dried under vacuum, and denoted as CeO₂-AA.

140 mg CeO₂-AA particles were then redispersed in 55 mL of distilled water, and 0.01 mmol metal precursor (H₂PtCl₆, PdCl₂, RhCl₃, RuCl₃) was added. After the mixture was stirred for 3 h at room temperature, the products were collected by centrifugation and washed with water several times. After being dried under vacuum, the products were calcinated at 300 °C in the air for 5 h to remove the excess AA and denoted as M₁/CeO₂.

Catalytic Methanol Steam Reforming. MSR over M₁/CeO₂ was performed in a continuous flow reactor. In a typical catalytic measurement, 100 mg of catalysts was mixed with 500 mg of white quartz (50–70 mesh particle size). Then the mixture was placed in a U-shaped fixed-bed flow reactor with an inner diameter of 4.50 mm, and the length of the catalyst bed is around 20 mm. Quartz wool was placed at both ends of the reactor. Helium (30 mL/min), regulated by a mass flow controller, was fed to the reactor at 1 atm. A methanol/water mixture (3 mL/h) with varying ratios (pure methanol, 1:1, 1:3, 1:5) was fed into the reactor by an injection pump. A K-type thermocouple was fixed at the center of the catalyst, and the temperature of bed was controlled by a PID 697 controller. The products were analyzed online by HP 5890 GC (HayeSep D column) equipped with a TCD detector.

The conversion of methanol and selectivity of CO₂ were calculated by the following equations

$$\text{Methanol Conversion}(\%) = \frac{\text{CO}_{\text{output}} + \text{CO}_2_{\text{output}}}{\text{Methanol}_{\text{input}}} \times 100\%$$

$$\text{CO}_2 \text{ Selectivity}(\%) = \frac{\text{CO}_2_{\text{output}}}{\text{CO}_{\text{output}} + \text{CO}_2_{\text{output}}} \times 100\%$$

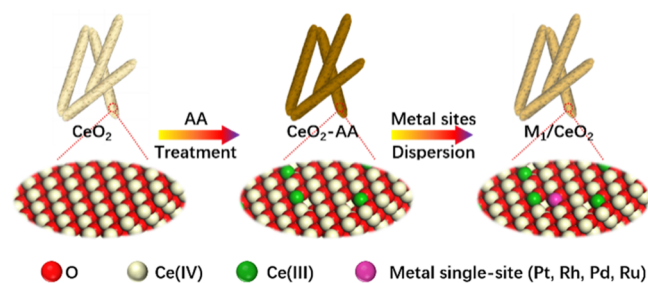
Catalytic Water Gas Shift (WGS) Reaction. The catalytic water gas shift (WGS) activities of M₁/CeO₂ catalysts were investigated using the same catalyst amounts in the same continuous flow reactor for MSR. He (28 mL/min) and CO (2 mL/min) were mixed and fed to the reactor at 1 atm, regulated by mass flow controllers. A flow of 2.25 mL/h of water was injected into the reactor. A K-type thermocouple was fixed in the center of catalysts, and the temperature of the bed was controlled by a PID 697 controller. The products were analyzed online by HP 5890 GC (HayeSep D column) equipped with a TCD detector.

Further details are available in the [Supporting Information](#).

RESULTS AND DISCUSSION

Synthesis and Characterization of M₁/CeO₂ Single-Site Catalysts. Ru₁/CeO₂ were fabricated by an AA-assisted reduction route ([Scheme 1](#)). The ascorbic acid was first

Scheme 1. Schematic Presentation of Synthesis Process for M₁/CeO₂ Single-Site Catalysts^a



^aM = Pt, Rh, Pd, Ru.

employed to create Ce³⁺ sites on the CeO₂ surface by reducing Ce⁴⁺. Then, prereduced CeO₂-AA was dispersed in the solution. After the addition of a ruthenium precursor (RuCl₃) solution, Ru was stabilized on the CeO₂ surface with the assistance of prereduced Ce³⁺ sites. After calcination in the air to remove the excess absorbed AA, the ruthenium single-sites were anchored on the CeO₂ support surface.

Powder X-ray diffraction (XRD) and high-resolution transmission electron microscope (TEM) were employed to identify the status of loaded Ru on CeO₂. XRD patterns ([Figure S1](#)) show no diffraction peaks attributed to metallic Ru due to the low concentration of Ru and its single-site status. Besides, compared to the original CeO₂ support ([Figure S2](#)), no apparent Ru nanoparticles or clusters were observed ([Figure 1a](#)) while the signals of Ru are uniformly distributed throughout CeO₂, as shown in the element mapping ([Figure 1b](#)). Extended X-ray absorption fine structure (EXAFS) further confirmed the atomic dispersion of ruthenium. As shown in [Figure 1d](#), only one notable peak attributed by Ru–O was observed in Fourier transformed (FT) *k*³-weighted EXAFS spectrum while the Ru–Ru peak was not detected ([Figure S3](#)), indicating isolated Ru sites were atomically dispersed on CeO₂ (detailed fitting parameters in [Table S1](#)).^{41,42} Besides, the X-ray absorption near-edge structure (XANES) spectrum of Ru₁/CeO₂ suggested ([Figure 1c](#)) that Ru atoms carry a positive charge (Ru^{δ+}) rather than Ru⁰. This was further investigated by

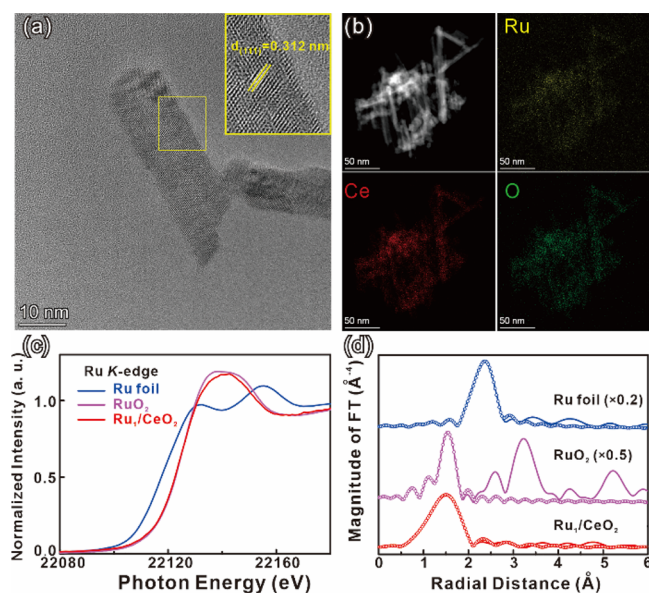


Figure 1. (a) High-resolution TEM image and (b) HAADF-STEM image and elemental mapping images of Ru₁/CeO₂ single-site catalyst. (c) Normalized XANES spectra of Ru₁/CeO₂, RuO₂, and bulk Ru foil at the Ru K-edge. (d) The k^3 -weighted Fourier transform EXAFS spectra with hollow points as fitting results.

CO adsorption and desorption using *in situ* diffuse reflectance infrared Fourier transform spectroscopy (DRIFTS) (Figure S4). Four peaks at 2173, 2117, 2045, and 1975 cm⁻¹ were detected, which is similar to those observed in reported Ru single-site catalysts.^{43,44} The peaks at 2045 and 1975 cm⁻¹ are attributed to the pair of bands of dicarbonyl species of CO adsorbed on oxidized Ru sites, Ru^{δ+}(CO)₂, while the peaks at 2173 and 2117 cm⁻¹ are ascribed to monocarbonyl species, Ru^{δ+}(CO), and tricarbonyl species, Ru^{δ+}(CO)₃, respectively.

The AA-assisted method can be extended to fabricate various CeO₂-supported noble metal single-site catalysts (i.e., Pt, Pd, and Rh) by simply replacing RuCl₃ with other metal precursors like H₂PtCl₆, PdCl₂, or RhCl₃. As shown in Figure 2, the noble metal elements are all uniformly distributed on CeO₂ without any nanoparticles or clusters detected (Figure S5; corresponding energy spectra are listed in Figure S6). EXAFS spectra in Figure 2 show peaks contributed by the metal–oxygen bond, confirming that the status of noble metal on CeO₂ are single sites. From the XANES spectrum (Figures S7–S9), all the metal atoms are in oxidized states rather than metallic states.

It has been reported that loading noble metal single-sites (e.g., Au, Pd, Rh, and Ru) onto CeO₂ can efficiently create oxygen vacancies near the dopant cations.^{19,45–47} Combined theoretical calculations and spectrum measurements have proven that the generated oxygen vacancies are located near the metal single sites, which created an ensemble reaction pool with the well-defined structure.⁴⁸ Synthetic methods such as atomic layer deposition (ALD) and impregnation-coprecipitation strategy would not involve the prereduction of the support, while our AA-assisted method can create more oxygen vacancies on the surface and thus have a higher chance to selectively immobilize metal single sites near the oxygen vacancy. According to XPS results (Figure S10, Table S2), the original proportion of Ce³⁺ in the shallows of as-synthesized CeO₂ is around 23.8%.⁴⁹ After AA reduction, the proportion of Ce³⁺ increased to 41.5%, indicating a lot of O vacancies were

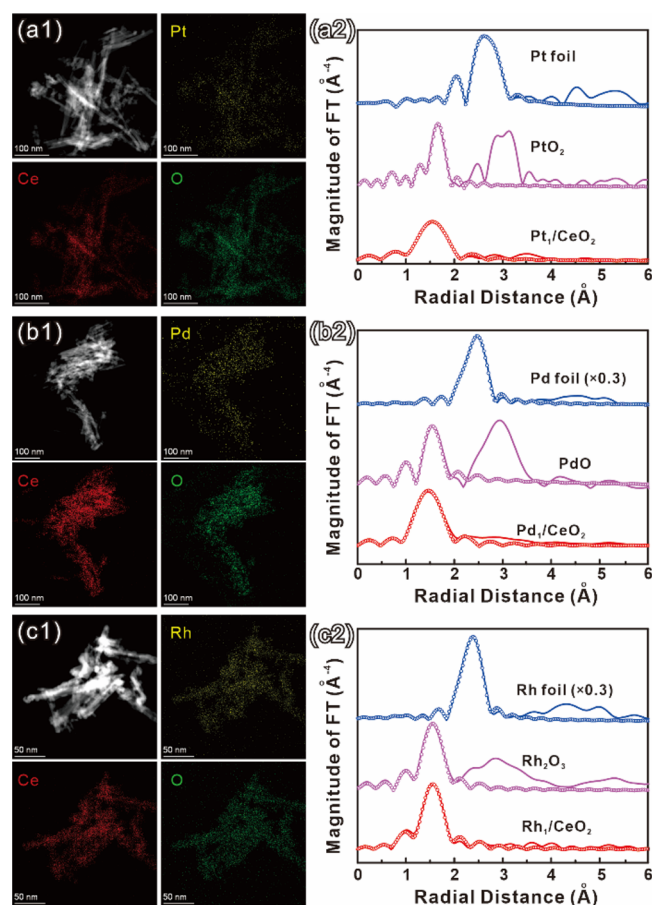


Figure 2. HAADF-STEM images and elemental mapping images of (a1) Pt₁/CeO₂, (b1) Pd₁/CeO₂, and (c1) Rh₁/CeO₂ single-site catalyst. (c) k^3 -weighted Fourier transform EXAFS spectra of (a2) Pt₁/CeO₂, (b2) Pd₁/CeO₂, (c2) Rh₁/CeO₂ and their relative metal foil and metal oxides.

created on the surface, which agreed with electron paramagnetic resonance (EPR) spectra and Raman spectra (Figure S11, 12).^{50,51} After air calcination to remove excess AA, the Ce³⁺ percentages of all M₁/CeO₂ decreased to a certain degree compared to CeO₂-AA, but they are still much higher than the original CeO₂ supports (Table S2). This result confirms that the introduction of metal single sites could further stabilize the neighboring oxygen vacancies, which is consistent with the prior report.⁵² Thus, more ensemble sites consisting of metal single site and surrounding oxygen vacancies were created via the AA-assisted method, which could be potentially applied in multistep tandem reactions.

Methanol Reforming over Ru₁/CeO₂ Single-Site Catalyst. Compared to methanol dehydrogenation, MSR not only releases 3 H₂ per methanol by utilizing the H₂ from water, achieving a high H₂ gravimetric density of 18.8%, but also avoids the generation of CO by the sequential WGS reaction.³¹ Significantly, the gas products of methanol steam reforming are H₂ and CO₂ without the poisoning gas CO, which can be potentially applied in the polymer electrolyte membrane fuel cells (PEMFCs) without any pretreatments.⁵²

We first investigated the catalytic performance of Ru₁/CeO₂ in both methanol dehydrogenation and MSR reactions using different ratios of methanol and water. As shown in Figure 3a,c, methanol dehydrogenation (black line labeled as 1:0) starts at 150 °C, and the higher reaction temperature favors the

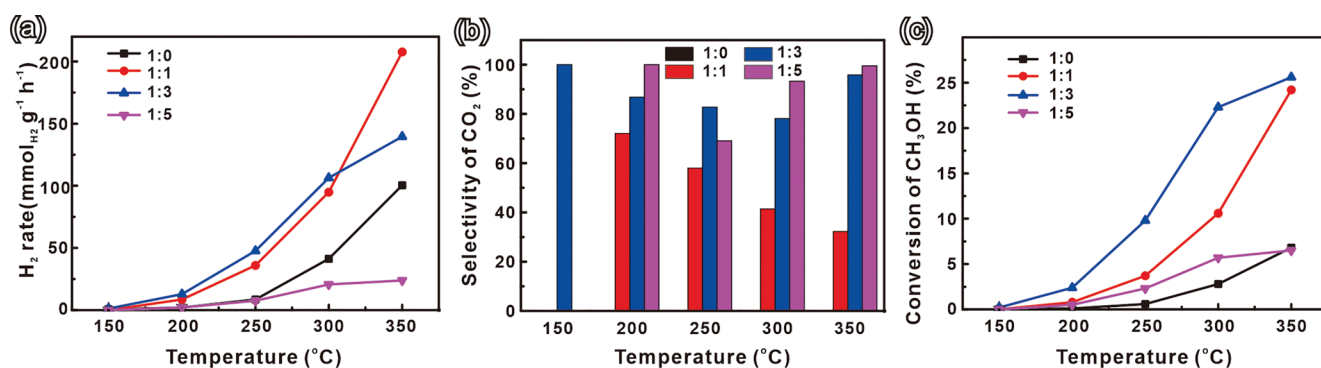


Figure 3. (a) Hydrogen generation rate, (b) CO₂ selectivity, and (c) methanol conversion of Ru₁/CeO₂ single-site catalyst at different temperatures with different ratios of methanol and water.

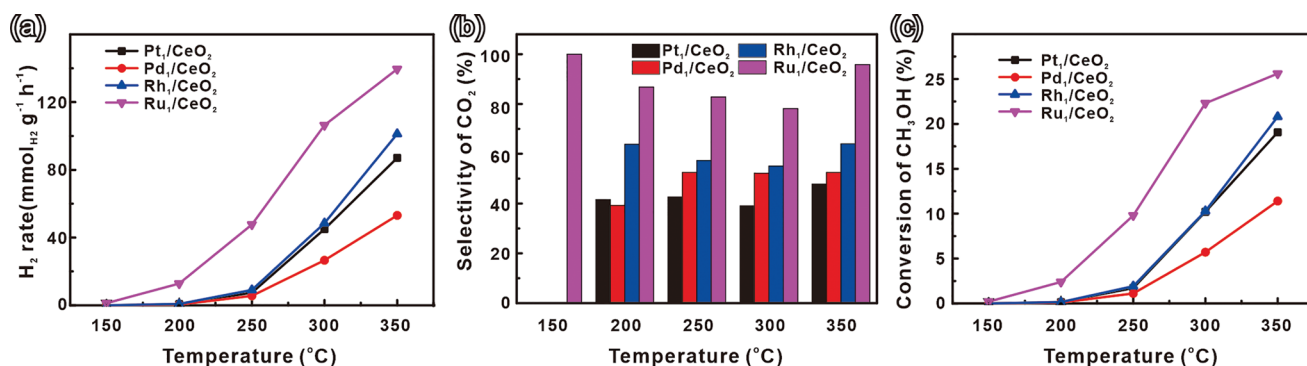


Figure 4. (a) Hydrogen generation rate, (b) CO₂ selectivity, and (c) methanol conversion of single-site M₁/CeO₂ catalysts at different temperatures with a 1:3 volume ratio of methanol and water.

methanol conversion. At 350 °C, the hydrogen production rate is 100.4 mmol_{H₂} g_{cat}⁻¹ h⁻¹ with a methanol conversion of 6.8%. The products of methanol dehydrogenation over Ru₁/CeO₂ only consist of H₂ and CO, and no formaldehyde was detected.

After the introduction of water vapor into the system, CO will further react with water through a sequential WGS reaction (CO + H₂O = CO₂ + H₂) over Ru₁/CeO₂. It will release one more H₂ and convert CO to CO₂. Compared to CO, CO₂ has a weaker bonding to the Ru single site, which can be easily removed under reaction condition to recover the active site for the next coming methanol. Therefore, introducing water could enhance the H₂ production as well as the conversion of methanol (Figures 3a,c). With water cofeed (V_{methanol}/V_{water} = 1:1), the hydrogen generation rate increased to 207.6 mmol_{H₂} g_{cat}⁻¹ h⁻¹ at 350 °C, which is two times that of pure methanol; 24.2% of methanol was converted, which is 4-fold that of direct methanol dehydrogenation without water. The selectivity of CO₂ in the product is about 32.2% (Figure 3b) under the methanol and water ratio of 1:1.

Further increase of the water/methanol ratio to 3:1 leads to the methanol conversion of 25.6% and 97.8% selectivity of CO₂ at 350 °C, due to the enhanced WGS reaction facilitated by the excess water. As the feeding rate of the water and methanol mixture is kept the same, less methanol was injected into the system. The lower methanol partial pressure decreases the generation rate of H₂ to 139.6 mmol_{H₂} g_{cat}⁻¹ h⁻¹ which is still higher than that of the pure methanol (100.4 mmol_{H₂} g_{cat}⁻¹ h⁻¹). It also ranks the highest among the reported noble metal catalysts in terms of CO₂ selectivity and H₂ generation rate (Figure S13). When compared with transition metal

catalysts such as Cu/ZnO-based catalysts, Ru₁/CeO₂ also had excellent activity and CO₂ selectivity in the temperature range of 150 to 350 °C (Table S3). Although the selectivity of CO₂ could increase to 99.5% at the water/methanol ratio of 5, the massive water vapor inhibited the methanol diffusion, leading to the lower H₂ generation rate of 23.8 mmol_{H₂} g_{cat}⁻¹ h⁻¹. Besides, at higher water concentrations (1:3 and 1:5), the relatively low methanol concentration will also slow down the growth of MSR rate at higher temperatures, because the methanol diffusion process was limited by a large amount of water molecules in the gas phase.

In practical application, the main issue hindering the application of single-site catalysts is their poor stability in the catalytic process, especially at operating temperature.⁵³ Therefore, the stability of Ru₁/CeO₂ was assessed in the catalytic reaction over time (Figure S14). The hydrogenation evolution rate was retained at 139.6 mmol_{H₂} g_{cat}⁻¹ h⁻¹ with more than 97% CO₂ selectivity within 72 h testing of methanol steam reforming at 350 °C (V_{methanol}/V_{water} = 1:3), indicating its excellent stability due to the strong interaction between Ru and CeO₂ surface.⁵⁴

Methanol Reforming on Different M₁/CeO₂ Single-Site Catalysts. We further investigated the catalytic performance of MSR (V_{methanol}/V_{water} = 1:3) over different M₁/CeO₂ catalysts (Ru₁/CeO₂, Rh₁/CeO₂, Pt₁/CeO₂, Pd₁/CeO₂) with a similar metal loading amount (0.14–0.15 wt %). For Pt₁/CeO₂, Rh₁/CeO₂, and Pd₁/CeO₂, only a small number of products were detected above 200 °C, of which the starting reaction temperature is higher than that of Ru₁/CeO₂ catalyst (150 °C). Similar to Ru₁/CeO₂, higher temperature favors the reforming reaction rate (Figure 4a,c). Under the same reaction

conditions and similar metal loading amount, Ru₁/CeO₂ showed the highest H₂ generation rate and methanol conversion with the activity order of Ru₁/CeO₂ > Rh₁/CeO₂ > Pt₁/CeO₂ > Pd₁/CeO₂.

More importantly, Ru₁/CeO₂ showed the highest CO₂ selectivity of 97.8% at 350 °C, while the other three single-site catalysts have only less than 60% CO₂ selectivity (Figure 4b). The catalytic results of MSR over M₁/CeO₂ showed that CO desorption and WGS are competing steps. Less CO desorption is the key to the higher selectivity of CO₂ in the subsequent WGS reaction. It has been reported that in comparison with Pt, Rh, and Pd, Ru has the lowest CO adsorption energy both for bulk materials and single-atom, indicating Ru has a much stronger bonding of CO.^{55,56} Therefore, CO-temperature-programmed desorption (CO-TPD) was then applied to investigate the strength of CO bonding on M₁/CeO₂ (Figure S15). The peak below 150 °C is attributed to CO adsorption on metal sites, while the peak between 200 to 300 °C is attributed to CO bonding on the CeO₂ support surface.^{57,58} Notably, different from other metals, Ru₁/CeO₂ displays a CO desorption peak around 350 °C, indicating the strong bonding between CO and Ru₁/CeO₂. In the reaction of methanol steam reforming, this strong interaction will further stabilize the CO intermediates, providing more chance for subsequent WGS reaction. On the other side, the single site Pt, Pd, and Rh do not have this strong bonding at 350 °C, so CO will desorb at lower temperatures, leading to decreased CO₂ selectivity.

Elementary-Step Methanol Dehydrogenation and WGS Reaction. MSR is a tandem reaction, including methanol dehydrogenation and the subsequent WGS reaction. Therefore, we carried out methanol dehydrogenation and WGS reaction over M₁/CeO₂ separately. As shown in Figure 5a, the methanol dehydrogenation catalyzed by different M₁/CeO₂ shows various H₂ generation rates. Methanol starts to dehydrogenate over Rh₁/CeO₂ and Pt₁/CeO₂ at a lower temperature of 150 °C, indicating superior activity toward Ru₁/CeO₂ and Pd₁/CeO₂. The H₂ generation rates at 350 °C

are in the order of Rh₁/CeO₂ (161.8 mmol_{H₂} g_{cat}⁻¹ h⁻¹) > Pt₁/CeO₂ (152.9 mmol_{H₂} g_{cat}⁻¹ h⁻¹) > Pd₁/CeO₂ (107.9 mmol_{H₂} g_{cat}⁻¹ h⁻¹) > Ru₁/CeO₂ (100.4 mmol_{H₂} g_{cat}⁻¹ h⁻¹). Interestingly, this activity trend is different from that of MSR in the presence of water, where H₂ generation rates are in the order of Ru₁/CeO₂ > Rh₁/CeO₂ > Pt₁/CeO₂ > Pd₁/CeO₂ (Figure 4a).

In the sequential WGS reaction (Figure 5c), Ru₁/CeO₂ has the highest activity from 200 to 350 °C. Especially at a lower temperature (200 °C), the CO conversion of Ru₁/CeO₂ (20.1%) is much higher than the other three catalysts, which are 7.5%, 0.9%, and 1.3% for Pt₁/CeO₂, Pd₁/CeO₂, Rh₁/CeO₂, respectively. The CO conversion of Ru₁/CeO₂ reached up to 100% at the high temperature (350 °C) while the WGS activity is in the order of Ru₁/CeO₂ > Pt₁/CeO₂ > Rh₁/CeO₂ > Pd₁/CeO₂.

The apparent activation energy (*E_a*) is a well-known empirical parameter in chemical kinetics that characterizes the dependence of the chemical rate coefficients on the temperature and provides information to compare the intrinsic activity of the catalysts.⁵⁹ We thus calculated the apparent activation energies for both reactions (Figure 5b,d) to understand the reaction mechanism and chemical kinetics. The activation energy of methanol dehydrogenation (*E_{a1}*) is in the order of Pt₁/CeO₂ (79.6 ± 6.2 kJ/mol) ≈ Rh₁/CeO₂ (81.4 ± 7.2 kJ/mol) < Ru₁/CeO₂ (94.0 ± 8.3 kJ/mol) < Pd₁/CeO₂ (102.3 ± 17.4 kJ/mol), while the activation energy of WGS reaction (*E_{a2}*) is in the order of Ru₁/CeO₂ (11.4 ± 0.7 kJ/mol) < Rh₁/CeO₂ (51.0 ± 5.4 kJ/mol) ≈ Pt₁/CeO₂ (51.9 ± 8.4 kJ/mol) ≈ Pd₁/CeO₂ (52.0 ± 8.6 kJ/mol). As reported, methanol steam reforming is a two-step reaction, where the activation energy of methanol dissociation (first step) is much higher than the subsequent WGS reaction (second step).³⁰ Meanwhile, the second step, WGS reaction, has a competing step: CO desorption. Therefore, the stronger CO adsorption and the lower *E_{a2}* of the WGS reaction could help the CO intermediates efficiently convert to CO₂ via the tandem reaction and recover more active sites for methanol dehydrogenation. Among all the studied single site catalysts, Ru₁/CeO₂ has an appropriate *E_{a1}* of methanol dehydrogenation, the lowest *E_{a2}* of WGS, and the strongest CO adsorption, resulting in the highest H₂ production rate and CO₂ selectivity. On the contrary, Pt₁/CeO₂ has the lowest *E_{a1}*, but its highest *E_{a2}*, and weak bonding with CO leading to the lowest CO₂ selectivity.

Proposed Reaction Mechanism. Combining our experimental findings and the insights provided by the preceding work, we proposed a reaction mechanism of tandem MSR reaction over M₁/CeO₂. As shown in Scheme 2, the methanol dehydrogenation occurs on the metal single site to release hydrogen and form the intermediate CO, where the neighboring O vacancies will facilitate the dissociative adsorption of methanol.²²

Depending on the binding strength, CO_{ad} would either desorb from the active sites and ends with a low CO₂ selectivity (i.e., Pt₁/CeO₂ case) or directly react with water to yield CO₂ via the sequential WGS reaction. Dissociation of water is generally considered a key step in WGS,^{60,61} and water molecules prefer to dissociate on the reduced CeO_x (O vacancy-Ce³⁺) by transferring a H atom to the neighboring surface oxygen.^{62,63} A recent study also revealed the synergistic effect between Pt sites and neighboring reduced Ce sites (Pt–O vacancy-Ce³⁺) at the interface of the Pt clusters and the

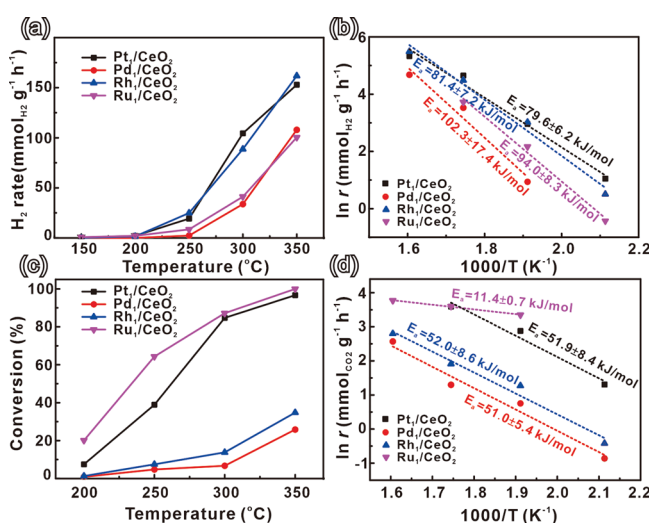
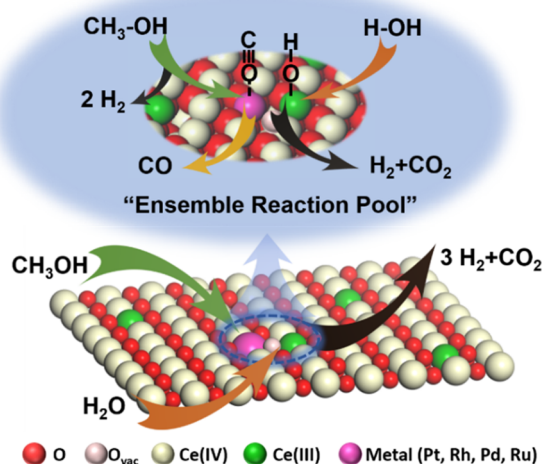


Figure 5. (a) H₂ generation rate over M₁/CeO₂ catalysts at different temperatures. (b) Arrhenius plots of methanol dehydrogenation over M₁/CeO₂ catalysts. (c) CO conversion of WGS over M₁/CeO₂ catalysts at different temperatures. (d) Arrhenius plots of WGS over M₁/CeO₂ catalysts.

Scheme 2. Proposed Reaction Pathway for Methanol Steam Reforming on M_1/CeO_2 Single-Site Catalysts



support,⁶⁴ and suggest only those oxygen vacancies nearby the Pt sites are involved in the WGS. M_1/CeO_2 in this work contains a similar structure, consisted of metal single sites with neighboring O vacancies (metal-O vacancy- Ce^{3+}). However, we could directly create much more “ensemble sites” using the AA-assisted synthetic approach, instead of a limited amount of active sites only at the interface of nanocluster and support, highlighting the great advantage of single-site catalysts. It has also been reported that the introduction of metal heteroatoms could efficiently create oxygen vacancy next to the dopant cations. Therefore, in our proposed “ensemble reaction pool”, the formed hydroxyl species adsorbed on the oxygen vacancy will react with the neighboring CO_{ad} , which avoids the diffusion process and lead to high activity.

CONCLUSION

In summary, the mechanism of methanol steam reforming tandem reaction was investigated over a series of CeO_2 -supported noble metal single site catalysts. Notably, Ru_1/CeO_2 displayed a much higher H_2 generation rate and CO_2 selectivity compared to those of the other three catalysts. Specifically, the stronger CO-metal bonding and larger difference of apparent activation energy between methanol dehydrogenation and WGS reaction resulted in the higher CO_2 selectivity. Importantly, different from metal nanoparticle catalysts, the metal single sites accompanied by the neighboring O vacancies generate an “ensemble reaction pool” to combine methanol dehydrogenation, water dissociation, and WGS reaction efficiently in the local environment. And this special synergy further improves the reaction efficiency and selectivity. Ultimately, this in-depth study highlights the benefits of well-designed single site catalysts for multiple step catalysis and paves the way for further rational design based on the “ensemble reaction pool” concept.

ASSOCIATED CONTENT

Supporting Information

The Supporting Information is available free of charge at <https://pubs.acs.org/doi/10.1021/jacs.1c03895>.

Experimental details, characterization data, and partial catalytic data, including the characterization of CeO_2

support, TEM images of M_1/CeO_2 catalyst, XPS spectra of CeO_2 and M_1/CeO_2 , EPR and Raman spectra of CeO_2 and CeO_2 -AA, CO adsorption–desorption DRIFTS of Ru_1/CeO_2 , CO-TPD results of M_1/CeO_2 catalysts, stability test of Ru_1/CeO_2 catalyst (PDF)

AUTHOR INFORMATION

Corresponding Authors

Ji Su – Chemical Sciences Division and Molecular Foundry, Lawrence Berkeley National Laboratory, Berkeley, California 94720, United States; Email: jisu@lbl.gov

Gabor A. Somorjai – Chemical Sciences Division, Lawrence Berkeley National Laboratory, Berkeley, California 94720, United States; Department of Chemistry, University of California-Berkeley, Berkeley, California 94720, United States; orcid.org/0000-0002-8478-2761; Email: somorjai@berkeley.edu

Authors

Luning Chen – Chemical Sciences Division, Lawrence Berkeley National Laboratory, Berkeley, California 94720, United States; State Key Laboratory of Physical Chemistry of Solid Surfaces, Collaborative Innovation Center of Chemistry for Energy Materials, and Department of Chemistry, College of Chemistry and Chemical Engineering, Xiamen University, Xiamen 361005, China; orcid.org/0000-0001-5434-4755

Zhiyuan Qi – Chemical Sciences Division, Lawrence Berkeley National Laboratory, Berkeley, California 94720, United States

Xinxing Peng – Chemical Sciences Division, Lawrence Berkeley National Laboratory, Berkeley, California 94720, United States; orcid.org/0000-0002-7077-8454

Jeng-Lung Chen – National Synchrotron Radiation Research Center, Hsinchu 30076, Taiwan

Chih-Wen Pao – National Synchrotron Radiation Research Center, Hsinchu 30076, Taiwan

Xibo Zhang – State Key Laboratory of Physical Chemistry of Solid Surfaces, Collaborative Innovation Center of Chemistry for Energy Materials, and Department of Chemistry, College of Chemistry and Chemical Engineering, Xiamen University, Xiamen 361005, China

Chaochao Dun – Molecular Foundry, Lawrence Berkeley National Laboratory, Berkeley, California 94720, United States; orcid.org/0000-0002-3215-6478

Melissa Young – Department of Chemistry, University of California-Berkeley, Berkeley, California 94720, United States

David Prendergast – Molecular Foundry, Lawrence Berkeley National Laboratory, Berkeley, California 94720, United States; orcid.org/0000-0003-0598-1453

Jeffrey J. Urban – Molecular Foundry, Lawrence Berkeley National Laboratory, Berkeley, California 94720, United States; orcid.org/0000-0002-6520-830X

Jinghua Guo – Advanced Light Source, Lawrence Berkeley National Laboratory, Berkeley, California 94720, United States; orcid.org/0000-0002-8576-2172

Complete contact information is available at:

<https://pubs.acs.org/doi/10.1021/jacs.1c03895>

Author Contributions

[§]L.C. and Z.Q. contributed equally to this work

Notes

The authors declare no competing financial interest.

■ ACKNOWLEDGMENTS

This work was supported by the Hydrogen Materials Advanced Research Consortium (HyMARC), established as part of the Energy Materials Network by the U.S. Department of Energy, Office of Energy Efficiency and Renewable Energy, Fuel Cell Technologies Office, under Contract Number DE-AC02-05CH11231, and Director, Office of Basic Energy Sciences, Division of Chemical Sciences, Geological and Biosciences of the U.S. Department of Energy under the same contract. This research used resources of the Advanced Light Source, which is a DOE Office of Science User Facility under the same contract. J. Guo, D. Prendergast, C. Dun, J. Urban and J. Su were supported by a User Project at The Molecular Foundry at Lawrence Berkeley National Laboratory, which is supported by the Office of Science of the U.S. Department of Energy under the same contract. L. Chen and Z. Qi acknowledge the financial support provided by catalysis research program DOE/LBNL DE-AC02-05CH11231, FWP no. CH030201.

■ REFERENCES

- (1) Kaiser, S. K.; Chen, Z.; Faust Akl, D.; Mitchell, S.; Pérez-Ramírez, J. Single-Atom Catalysts across the Periodic Table. *Chem. Rev.* **2020**, *120*, 11703–11809.
- (2) Ji, S.; Chen, Y.; Wang, X.; Zhang, Z.; Wang, D.; Li, Y. Chemical synthesis of single atomic site catalysts. *Chem. Rev.* **2020**, *120*, 11900–11955.
- (3) Lang, R.; Du, X.; Huang, Y.; Jiang, X.; Zhang, Q.; Guo, Y.; Liu, K.; Qiao, B.; Wang, A.; Zhang, T. Single-Atom Catalysts Based on the Metal-Oxide Interaction. *Chem. Rev.* **2020**, *120*, 11986–12043.
- (4) Kistler, J. D.; Chotigkrai, N.; Xu, P.; Enderle, B.; Praserthdam, P.; Chen, C. Y.; Browning, N. D.; Gates, B. C. A single-site platinum CO oxidation catalyst in zeolite KLTL: microscopic and spectroscopic determination of the locations of the platinum atoms. *Angew. Chem., Int. Ed.* **2014**, *53*, 8904–8907.
- (5) Rascón, F.; Wischert, R.; Copéret, C. Molecular nature of support effects in single-site heterogeneous catalysts: silica vs. alumina. *Chem. Sci.* **2011**, *2*, 1449–1456.
- (6) Thomas, J. M.; Raja, R.; Lewis, D. W. Single-site heterogeneous catalysts. *Angew. Chem., Int. Ed.* **2005**, *44*, 6456–6482.
- (7) Qiao, B.; Wang, A.; Yang, X.; Allard, L. F.; Jiang, Z.; Cui, Y.; Liu, J.; Li, J.; Zhang, T. Single-atom catalysis of CO oxidation using Pt₁/FeOx. *Nat. Chem.* **2011**, *3*, 634–641.
- (8) Jones, J.; Xiong, H.; DeLaRiva, A. T.; Peterson, E. J.; Pham, H.; Challa, S. R.; Qi, G.; Oh, S.; Wiebenga, M. H.; Hernández, X. I. P.; Wang, Y. Thermally stable single-atom platinum-on-ceria catalysts via atom trapping. *Science* **2016**, *353*, 150–154.
- (9) Wang, L.; Zhang, W.; Wang, S.; Gao, Z.; Luo, Z.; Wang, X.; Zeng, R.; Li, A.; Li, H.; Wang, M.; Zheng, X. Atomic-level insights in optimizing reaction paths for hydroformylation reaction over Rh/CoO single-atom catalyst. *Nat. Commun.* **2016**, *7*, 1–8.
- (10) Lee, B. H.; Park, S.; Kim, M.; Sinha, A. K.; Lee, S. C.; Jung, E.; Chang, W. J.; Lee, K. S.; Kim, J. H.; Cho, S. P.; Kim, H. Reversible and cooperative photoactivation of single-atom Cu/TiO₂ photocatalysts. *Nat. Mater.* **2019**, *18*, 620–626.
- (11) Liu, P.; Zhao, Y.; Qin, R.; Mo, S.; Chen, G.; Gu, L.; Chevrier, D. M.; Zhang, P.; Guo, Q.; Zang, D.; Wu, B. Photochemical route for synthesizing atomically dispersed palladium catalysts. *Science* **2016**, *352*, 797–800.
- (12) Nie, L.; Mei, D.; Xiong, H.; Peng, B.; Ren, Z.; Hernandez, X. I. P.; DeLaRiva, A.; Wang, M.; Engelhard, M. H.; Kovarik, L.; Datye, A. K. Activation of surface lattice oxygen in single-atom Pt/CeO₂ for low-temperature CO oxidation. *Science* **2017**, *358*, 1419–1423.
- (13) Lin, J.; Wang, A.; Qiao, B.; Liu, X.; Yang, X.; Wang, X.; Liang, J.; Li, J.; Liu, J.; Zhang, T. Remarkable performance of Ir₁/FeOx single-atom catalyst in water gas shift reaction. *J. Am. Chem. Soc.* **2013**, *135*, 15314–15317.
- (14) Shan, J.; Li, M.; Allard, L. F.; Lee, S.; Flytzani-Stephanopoulos, M. Mild oxidation of methane to methanol or acetic acid on supported isolated rhodium catalysts. *Nature* **2017**, *551*, 605–608.
- (15) Jeong, H.; Kwon, O.; Kim, B. S.; Bae, J.; Shin, S.; Kim, H. E.; Kim, J.; Lee, H. Highly durable metal ensemble catalysts with full dispersion for automotive applications beyond single-atom catalysts. *Nat. Catal.* **2020**, *3*, 368–375.
- (16) Jeong, H.; Lee, G.; Kim, B. S.; Bae, J.; Han, J. W.; Lee, H. Fully dispersed Rh ensemble catalyst to enhance low-temperature activity. *J. Am. Chem. Soc.* **2018**, *140*, 9558–9565.
- (17) Jeong, H.; Shin, S.; Lee, H. Heterogeneous Atomic Catalysts Overcoming the Limitations of Single-Atom Catalysts. *ACS Nano* **2020**, *14*, 14355–14374.
- (18) Wang, L.; Guan, E.; Zhang, J.; Yang, J.; Zhu, Y.; Han, Y.; Yang, M.; Cen, C.; Fu, G.; Gates, B. C.; Xiao, F. S. Single-site catalyst promoters accelerate metal-catalyzed nitroarene hydrogenation. *Nat. Commun.* **2018**, *9*, 1–8.
- (19) Li, T.; Liu, F.; Tang, Y.; Li, L.; Miao, S.; Su, Y.; Zhang, J.; Huang, J.; Sun, H.; Haruta, M.; Wang, A. Maximizing the number of interfacial sites in single-atom catalysts for the highly selective, solvent-free oxidation of primary alcohols. *Angew. Chem., Int. Ed.* **2018**, *57*, 7795–7799.
- (20) Yu, K.; Lou, L. L.; Liu, S.; Zhou, W. Asymmetric oxygen vacancies: the intrinsic redox active sites in metal oxide catalysts. *Adv. Sci.* **2020**, *7*, 1901970.
- (21) Chen, L. N.; Hou, K. P.; Liu, Y. S.; Qi, Z. Y.; Zheng, Q.; Lu, Y. H.; Chen, J. Y.; Chen, J. L.; Pao, C. W.; Wang, S. B.; Li, Y. B.; et al. Efficient hydrogen production from methanol using a single-site Pt₁/CeO₂ catalyst. *J. Am. Chem. Soc.* **2019**, *141*, 17995–17999.
- (22) Qi, Z.; Chen, L.; Zhang, S.; Su, J.; Somorjai, G. A. Mechanism of Methanol Decomposition over Single-Site Pt₁/CeO₂ Catalyst: A DRIFTS Study. *J. Am. Chem. Soc.* **2021**, *143*, 60–64.
- (23) Zhang, S.; Chen, L.; Qi, Z.; Zhuo, L.; Chen, J. L.; Pao, C. W.; Su, J.; Somorjai, G. A. Insights into the Mechanism of n-Hexane Reforming over a Single-Site Platinum Catalyst. *J. Am. Chem. Soc.* **2020**, *142*, 16533–16537.
- (24) Tromp, T. K.; Shia, R. L.; Allen, M.; Eiler, J. M.; Yung, Y. L. Potential environmental impact of a hydrogen economy on the stratosphere. *Science* **2003**, *300*, 1740–1742.
- (25) Muradov, N. Z.; Veziroğlu, T. N. Green” path from fossil-based to hydrogen economy: an overview of carbon-neutral technologies. *Int. J. Hydrogen Energy* **2008**, *33*, 6804–6839.
- (26) Muradov, N. Z.; Veziroğlu, T. N. From hydrocarbon to hydrogen-carbon to hydrogen economy. *Int. J. Hydrogen Energy* **2005**, *30*, 225–237.
- (27) Liu, W. C.; Baek, J.; Somorjai, G. A. The methanol economy: methane and carbon dioxide conversion. *Top. Catal.* **2018**, *61*, 530–541.
- (28) Wang, T.; Chen, Z. X.; Yu, S.; Sheng, T.; Ma, H. B.; Chen, L. N.; Rauf, M.; Xia, H. P.; Zhou, Z. Y.; Sun, S. G. Constructing canopy-shaped molecular architectures to create local Pt surface sites with high tolerance to H₂S and CO for hydrogen electrooxidation. *Energy Environ. Sci.* **2018**, *11*, 166–171.
- (29) Nilekar, A. U.; Sasaki, K.; Farberow, C. A.; Adzic, R. R.; Mavrikakis, M. Mixed-metal Pt monolayer electrocatalysts with improved CO tolerance. *J. Am. Chem. Soc.* **2011**, *133*, 18574–18576.
- (30) Iulianelli, A.; Ribeirinha, P.; Mendes, A.; Basile, A. Methanol steam reforming for hydrogen generation via conventional and membrane reactors: a review. *Renewable Sustainable Energy Rev.* **2014**, *29*, 355–368.
- (31) Palo, D. R.; Dagle, R. A.; Holladay, J. D. Methanol steam reforming for hydrogen production. *Chem. Rev.* **2017**, *107*, 3992–4021.
- (32) Lin, L.; Zhou, W.; Gao, R.; Yao, S.; Zhang, X.; Xu, W.; Zheng, S.; Jiang, Z.; Yu, Q.; Li, Y. W.; Shi, C. Low-temperature hydrogen production from water and methanol using Pt/ α -MoC catalysts. *Nature* **2017**, *544*, 80–83.

- (33) Lin, L.; Yu, Q.; Peng, M.; Li, A.; Yao, S.; Tian, S.; Liu, X.; Li, A.; Jiang, Z.; Gao, R.; Han, X.; et al. Atomically Dispersed Ni/ α -MoC Catalyst for Hydrogen Production from Methanol/Water. *J. Am. Chem. Soc.* **2021**, *143* (1), 309–317.
- (34) Yamada, Y.; Tsung, C. K.; Huang, W.; Huo, Z.; Habas, S. E.; Soejima, T.; Aliaga, C. E.; Somorjai, G. A.; Yang, P. Nanocrystal bilayer for tandem catalysis. *Nat. Chem.* **2011**, *3*, 372–376.
- (35) Rayder, T. M.; Adillon, E. H.; Byers, J. A.; Tsung, C. K. A Bioinspired Multicomponent Catalytic System for Converting Carbon Dioxide into Methanol Autocatalytically. *Chem.* **2020**, *6*, 1742–1754.
- (36) Ma, H.; Ma, G.; Qi, Y.; Wang, Y.; Chen, Q.; Rout, K. R.; Fuglerud, T.; Chen, D. Nitrogen-Doped Carbon-Assisted One-pot Tandem Reaction for Vinyl Chloride Production via Ethylene Oxychlorination. *Angew. Chem., Int. Ed.* **2020**, *59*, 22080–22085.
- (37) Cho, H. J.; Kim, D.; Li, J.; Su, D.; Xu, B. Zeolite-encapsulated Pt nanoparticles for tandem catalysis. *J. Am. Chem. Soc.* **2018**, *140*, 13514–13520.
- (38) Chen, L.; Zhang, X.; Zhou, J.; Xie, Z.; Kuang, Q.; Zheng, L. A nano-reactor based on PtNi@ metal–organic framework composites loaded with polyoxometalates for hydrogenation–esterification tandem reactions. *Nanoscale* **2019**, *11*, 3292–3299.
- (39) Su, J.; Xie, C.; Chen, C.; Yu, Y.; Kennedy, G.; Somorjai, G. A.; Yang, P. Insights into the mechanism of tandem alkene hydroformylation over a nanostructured catalyst with multiple interfaces. *J. Am. Chem. Soc.* **2016**, *138*, 11568–11574.
- (40) Mai, H. X.; Sun, L. D.; Zhang, Y. W.; Si, R.; Feng, W.; Zhang, H. P.; Liu, H. C.; Yan, C. H. Shape-selective synthesis and oxygen storage behavior of ceria nanopolyhedra, nanorods, and nanocubes. *J. Phys. Chem. B* **2005**, *109*, 24380–24385.
- (41) Ravel, B.; Newville, M. A.T.H.E.N.A. ATHENA, ARTEMIS, HEPHAESTUS: data analysis for X-ray absorption spectroscopy using IFEFFIT. *J. Synchrotron Radiat.* **2005**, *12*, 537–541.
- (42) Sarma, B. B.; Kim, J.; Amsler, J.; Agostini, G.; Weidenthaler, C.; Pfänder, N.; Arenal, R.; Concepción, P.; Plessow, P.; Studt, F.; Prieto, G. One-pot cooperation of single-atom Rh and Ru solid catalysts for a selective tandem olefin isomerization-hydrosilylation process. *Angew. Chem., Int. Ed.* **2020**, *59*, 5806–5815.
- (43) Thang, H. V.; Tosoni, S.; Fang, L.; Bruijninx, P.; Pacchioni, G. Nature of Sintering-Resistant, Single-Atom Ru Species Dispersed on Zirconia-Based Catalysts: A DFT and FTIR Study of CO Adsorption. *ChemCatChem* **2018**, *10*, 2634–2645.
- (44) Qiu, J. Z.; Hu, J.; Lan, J.; Wang, L. F.; Fu, G.; Xiao, R.; Ge, B.; Jiang, J. Pure Siliceous Zeolite-Supported Ru Single-Atom Active Sites for Ammonia Synthesis. *Chem. Mater.* **2019**, *31*, 9413–9421.
- (45) Fu, Q.; Saltsburg, H.; Flytzani-Stephanopoulos, M. Active nonmetallic Au and Pt species on ceria-based water-gas shift catalysts. *Science* **2003**, *301*, 935–938.
- (46) Shapovalov, V.; Metiu, H. Catalysis by doped oxides: CO oxidation by $\text{Au}_x\text{Ce}_{1-x}\text{O}_2$. *J. Catal.* **2007**, *245*, 205–214.
- (47) Tang, W.; Hu, Z.; Wang, M.; Stucky, G. D.; Metiu, H.; McFarland, E. W. Methane complete and partial oxidation catalyzed by Pt-doped CeO_2 . *J. Catal.* **2010**, *273*, 125–137.
- (48) Liu, C.; Chen, Z.; Yan, H.; Xi, S.; Yam, K. M.; Gao, J.; Du, Y.; Li, J.; Zhao, X.; Xie, K.; Xu, H. Expedient synthesis of E-hydrazone esters and 1H-indazole scaffolds through heterogeneous single-atom platinum catalysis. *Sci. Adv.* **2019**, *5*, 1537.
- (49) Chen, J.; Wanyan, Y.; Zeng, J.; Fang, H.; Li, Z.; Dong, Y.; Qin, R.; Wu, C.; Liu, D.; Wang, M.; Kuang, Q.; Xie, Z.; Zheng, L. Surface engineering protocol to obtain an atomically dispersed Pt/ CeO_2 catalyst with high activity and stability for CO oxidation. *ACS Sustainable Chem. Eng.* **2018**, *6*, 14054–14062.
- (50) Khan, M. E.; Khan, M. M.; Cho, M. H. Ce^{3+} -ion, surface oxygen vacancy, and visible light-induced photocatalytic dye degradation and photocapacitive performance of CeO_2 -graphene nanostructures. *Sci. Rep.* **2017**, *7*, 1–17.
- (51) Lykaki, M.; Pachatouridou, E.; Carabineiro, S. A.; Iliopoulou, E.; Andriopoulou, C.; Kallithrakas-Kontos, N.; Boghosian, S.; Konsolakis, M. Ceria nanoparticles shape effects on the structural defects and surface chemistry: Implications in CO oxidation by Cu/ CeO_2 catalysts. *Appl. Catal., B* **2018**, *230*, 18–28.
- (52) McFarland, E. W.; Metiu, H. Catalysis by doped oxides. *Chem. Rev.* **2013**, *113*, 4391–4427.
- (53) Duan, S.; Wang, R.; Liu, J. Stability investigation of a high number density Pt₁/Fe₂O₃ single-atom catalyst under different gas environments by HAADF-STEM. *Nanotechnology* **2018**, *29*, 204002.
- (54) Liu, J. C.; Tang, Y.; Wang, Y. G.; Zhang, T.; Li, J. Theoretical understanding of the stability of single-atom catalysts. *Natl. Sci. Rev.* **2018**, *5*, 638–641.
- (55) Abild-Pedersen, F.; Andersson, M. P. CO adsorption energies on metals with correction for high coordination adsorption sites—A density functional study. *Surf. Sci.* **2007**, *601*, 1747–1753.
- (56) Sarma, B. B.; Plessow, P. N.; Agostini, G.; Concepción, P.; Pfänder, N.; Kang, L.; Wang, F. R.; Studt, F.; Prieto, G. Metal-specific reactivity in single-atom catalysts: CO oxidation on 4d and 5d transition metals atomically dispersed on MgO. *J. Am. Chem. Soc.* **2020**, *142*, 14890–14902.
- (57) Wu, Z.; Li, M.; Overbury, S. H. On the Structure Dependence of CO Oxidation over CeO_2 nanocrystals with Well-Defined Surface Planes. *J. Catal.* **2012**, *285*, 61–73.
- (58) Zhu, H. O.; Kim, J. R.; Ihm, S. K. Characteristics of Pt/ WO_3 / CeO_2 / ZrO_2 Catalysts for Catalytic Reduction of NO by CO. *Appl. Catal., B* **2009**, *86*, 87–92.
- (59) Calderón-Cárdenas, A.; Paredes-Salazar, E. A.; Varela, H. Apparent Activation Energy in Electrochemical Multistep Reactions: A Description via Sensitivities and Degrees of Rate Control. *ACS Catal.* **2020**, *10*, 9336–9345.
- (60) Song, W.; Hensen, E. J. Mechanistic aspects of the water–gas shift reaction on isolated and clustered Au atoms on CeO_2 (110): A density functional theory study. *ACS Catal.* **2014**, *4*, 1885–1892.
- (61) Vecchiotti, J.; Bonivardi, A.; Xu, W.; Stacchiola, D.; Delgado, J. J.; Calatayud, M.; Collins, S. E. Understanding the role of oxygen vacancies in the water gas shift reaction on ceria-supported platinum catalysts. *ACS Catal.* **2014**, *4*, 2088–2096.
- (62) Vovchok, D.; Guild, C. J.; Dissanayake, S.; Llorca, J.; Stavitski, E.; Liu, Z.; Palomino, R. M.; Waluyo, I.; Li, Y.; Frenkel, A. I.; Rodriguez, J. A. In situ characterization of mesoporous Co/ CeO_2 catalysts for the high-temperature water-gas shift. *J. Phys. Chem. C* **2018**, *122*, 8998–9008.
- (63) Aranifard, S.; Ammal, S. C.; Heyden, A. On the importance of metal–oxide interface sites for the water–gas shift reaction over Pt/ CeO_2 catalysts. *J. Catal.* **2014**, *309*, 314–324.
- (64) Li, Y.; Kottwitz, M.; Vincent, J. L.; Enright, M. J.; Liu, Z.; Zhang, L.; Huang, J.; Senanayake, S. D.; Yang, W. C. D.; Crozier, P. A.; Nuzzo, R. G. Dynamic structure of active sites in ceria-supported Pt catalysts for the water gas shift reaction. *Nat. Commun.* **2021**, *12*, 1–9.